HDL-TR-2166

Down-Range Imaging of Radar Targets

by Joseph D. Silverstein

The findings in this report are not to be construed as an official Department of the Army position unless so designated by other authorized documents.

Citation of manufacturer's or trade names does not constitute an official endorsement or approval of the use thereof.

Destroy this report when it is no longer needed. Do not return it to the originator.

(2)

UNCLASSIFIED

SECURITY CLASSIFICATION OF THIS PAGE

REPORT DOCUMENTATION PAGE

Form Approved
OMB No. 0704-0188

1a. REPORT SECURITY CLASSIFICATION: Unclassified	1b. RESTRICTIVE MARKINGS
2a. SECURITY CLASSIFICATION AUTHORITY	3. DISTRIBUTION/AVAILABILITY OF REPORT: Approved for public release; distribution unlimited.
2b. DECLASSIFICATION/DOWNGRADING SCHEDULE	
4. PERFORMING ORGANIZATION REPORT NUMBER(S): HDL-TR-2166	5. MONITORING ORGANIZATION REPORT NUMBER(S)
6a. NAME OF PERFORMING ORGANIZATION: Harry Diamond Laboratories; 6b. OFFICE SYMBOL (if applicable): SLCHD-ST-SP	7a. NAME OF MONITORING ORGANIZATION
6c. ADDRESS (City, State, and ZIP Code): 2800 Powder Mill Road, Adelphi, MD 20783-1197	7b. ADDRESS (City, State, and ZIP Code)
8a. NAME OF FUNDING/SPONSORING ORGANIZATION: U.S. Army Laboratory Command; 8b. OFFICE SYMBOL (if applicable): AMSLC	9. PROCUREMENT INSTRUMENT IDENTIFICATION NUMBER
8c. ADDRESS (City, State, and ZIP Code): 2800 Powder Mill Road, Adelphi, MD 20783-1145	10. SOURCE OF FUNDING NUMBERS: PROGRAM ELEMENT NO. 612120.H1600; PROJECT NO. AH16; TASK NO.; WORK UNIT ACCESSION NO

11. TITLE (Include Security Classification): Down-Range Imaging of Radar Targets

12. PERSONAL AUTHOR(S): Joseph D. Silverstein

13a. TYPE OF REPORT	13b. TIME COVERED	14. DATE OF REPORT (Year, Month, Day)	15. PAGE COUNT
Final	FROM 1986 TO 1988	January 1990	51

16. SUPPLEMENTARY NOTATION: AMS code: 612120.H1611, HDL project: 1E2813

17. COSATI CODES			18. SUBJECT TERMS (Continue on reverse if necessary and identify by block number)
FIELD	GROUP	SUB-GROUP	Down-range resolution, resolution cell, discrete Fourier transform, point-reflector target
17	09		
17	07		

19. ABSTRACT (Continue on reverse if necessary and identify by block number)

A derivation is given of the one-dimensional, down-range image of a radar target in terms of the discrete Fourier transform (DFT) of the target returns at each of a number of equally spaced radar frequencies. The formula for the image is applied to return signals computed for point targets. In general, as long as the points are separated by at least 1.5 resolution cell widths, and their reflectivities differ by no more than a factor of 2, the images yield fairly accurate information on both the relative location and reflectivity of the points of the target.

20. DISTRIBUTION/AVAILABILITY OF ABSTRACT: ☒ UNCLASSIFIED/UNLIMITED ☐ SAME AS RPT ☐ DTIC USERS	21. ABSTRACT SECURITY CLASSIFICATION: Unclassified
22a. NAME OF RESPONSIBLE INDIVIDUAL: Joseph D. Silverstein	22b. TELEPHONE (Include Area Code): (202) 394-3170; 22c. OFFICE SYMBOL: SLCHD-ST-SP

DD Form 1473, JUN 86 — Previous editions are obsolete. — SECURITY CLASSIFICATION OF THIS PAGE: UNCLASSIFIED

Contents

Figures

Table

1. Introduction

Much progress has been made in the development of wide-bandwidth, highly coherent, polarization-agile, millimeter-wave radars to aid in the design and testing of smart munitions. These radars employ modern signal-processing schemes to achieve spatial resolution of discrete electromagnetic scatterers contained in the target and/or background by means of Fourier analysis. A basic understanding of how such resolution is achieved by this method is therefore necessary if we wish to optimally design and/or evaluate signal-processing algorithms for these radars. It is toward that goal that this report is addressed.

The report develops one-dimensional, down-range imaging techniques and applies them to point targets. Because the Fourier-analytical tools involved in the study of these relatively simple cases require only a minimum of mathematical manipulation, a clear understanding is obtained of how the image might be significantly altered by slight changes in the radar frequency, radar-to-target distance, and relative positioning of the target point reflectors. The techniques described in this report underlie the achievement of cross-range as well as down-range resolution of more complicated targets embedded in background, when there is motion of the radar relative to the target, or vice versa, through the synthetic aperture radar (SAR) or inverse synthetic aperture radar (ISAR) techniques.[1] ISAR is an especially important technique, since it is used extensively to generate data useful for evaluating various target discrimination and tracking schemes currently being proposed.

[1] *R. N. Trebits,* ***Synthetic Aperture Radar****, in* ***Principles of Modern Radar****, J. L. Eaves and E. K. Reedy, eds, Van Nostrand Reinhold (1987), pp 502–537.*

2. Returned Signals of Stepped Frequency Radar

Assume a cw radar illuminates an *isolated* target of finite extent in the down-range direction, i.e., along the radar line of sight (RLOS), with plane monochromatic waves. This is the very idealized case of a target located very far from a radar which transmits spherical waves. Assume that the radar is coherent; that is, it can measure both the amplitude and the phase of the returned signal relative to those of some reference signal identical to the transmitted signal.

We use the following notation:

f = frequency of waves, in hertz,
X, x = down-range coordinate of sampled point and target point, in meters,
$G(x)$ = reflectivity density function (generally complex), in meters^{-1},
$v(f)$ = ratio of return field strength at frequency f impinging on the detector to field strength at f illuminating the target (generally complex),
c = velocity of light, in meters per second,
x_a = smallest down-range coordinate of target, in meters,
x_b = largest down-range coordinate of target, in meters, and
L = $x_b - x_a$ = down-range extent of target, in meters.

Make the following assumptions:

a. The round-trip atmospheric attenuation of the waves is negligible.
b. The entire target is illuminated by the plane waves so that all cross-range effects are "averaged out."

Under these conditions

$$v(f) = \int_{x_a}^{x_b} G(x)\, e^{i2\pi f(2x)/c}\, dx \quad , \tag{1}$$

where the factor 2 multiplying x in the phase exponent accounts for the fact that the waves make a round trip.

Let the radar illuminate the target with a sequence of N_f waves of frequency f_n, where

$$n = 0, 1, 2 \ldots, N_f - 1 \quad ,$$

equally spaced by Δf Hz and with a lowest value of f_0 Hz. Thus

$$f_n = f_0 + n\Delta f \quad . \tag{2}$$

If v_n is the return signal at f_n, then from equation (1)

$$v_n = \int_{x_a}^{x_b} G(x)\; e^{i2\pi f_n(2x)/c}\, dx \quad . \tag{3}$$

3. Derivation of Down-Range Image[2]

We consider a "sampling length," R, which is given by

$$R = \frac{c}{2\Delta f} \quad . \tag{4}$$

We in turn divide R into N_f sampling cells of length ΔX, so that

$$\Delta X = \frac{R}{N_f} = \frac{c}{2N_f \Delta f} \quad . \tag{5}$$

We further assume that the entire target is located within an interval, called a "sampling interval," which extends from X_0 to $X_0 + R$, where

$$X_0 = M N_f \Delta X = \frac{Mc}{2\Delta f} \tag{6}$$

with M an *integer*. Thus, the left boundary of the k^{th} cell ($k = 0, 1, 2, \ldots, N_f - 1$) is $X_0 + k\Delta X$, and its right boundary is $X_0 + (k + 1)\Delta X$. The case of a target spanning two neighboring sampling intervals is treated in section 5.

Let

$$G(X) = G(x) \quad , \; x_a \le X \le x_b \quad ,$$
$$G(X) = 0 \qquad , \text{ otherwise} \quad .$$

We define the k^{th} sample of $G(X)$ as

$$g_k \equiv \int_{X_0 + k\Delta X}^{X_0 + (k+1)\Delta X} G(X)\, dX \quad . \tag{7}$$

We consider approximating $G(X)$ by a sum of "impulses" of height g_k at the left cell-boundary points:

[2] *Many general concepts and mathematical techniques related to obtaining both down-range and cross-range resolution are discussed by Dean L. Mensa in* ***High Resolution Radar Imaging****, Artech House (1981).*

$$X_k = X_0 + k\Delta X \quad . \tag{8}$$

Thus

$$G(X) \equiv g(X) = \sum_{k=0}^{N_f-1} g_k \delta(X - X_k) \quad , \tag{9}$$

where $\delta(X)$ is the delta function. This function has the property that

$$\begin{aligned} &\int_a^b f(X)\,\delta(X - X_0)\; dX \equiv f(X_0) \quad , \text{ if } (a,b) \text{ contains } X_0 \quad , \\ &\int_a^b f(X)\,\delta(X - X_0)\; dX \equiv 0 \qquad\quad , \text{ otherwise} \quad , \end{aligned} \tag{10}$$

for any analytic function $f(X)$ uniquely defined at X_0. Equation (9) then yields an approximate form for v_n in equation (3):

$$v_n = \sum_{k=0}^{N_f-1} g_k e^{i2\pi f_n 2X_k/c} \quad . \tag{11}$$

One expects the accuracy of the above expression to depend on how well the target function $G(X)$ can be represented as in equation (9), that is, by a series of isolated high-reflectivity points separated by ΔX. In effect, equation (11) represents an approximation to the function $v(f)$ in equation (1), which can be viewed as the Fourier transform of the target function $G(x)$ in spatial frequency space.

If we define the ratio of f_0 to Δf as P, i.e.,

$$P \equiv f_0/\Delta f \quad . \tag{12}$$

substitute equations (5), (6), (8), and (12) into equation (11), and note that $e^{i2\pi nM} = 1$, the result is

$$v_n e^{-i2\pi PM} = \sum_{k=0}^{N_f-1} \left(g_k e^{i2\pi Pk/N_f} \right) e^{i2\pi nk/N_f} \quad . \tag{13}$$

The inverse relation of the above equation is

$$g_k e^{i2\pi Pk/N_f} = \frac{e^{-i2\pi PM}}{N_f} \sum_{n=0}^{N_f-1} v_n e^{-i2\pi nk/N_f} \quad . \tag{14}$$

Equation (14) is the forward discrete Fourier transform (DFT)[3,4] relation between the sequences $v_n e^{-i2\pi PM}$ and $g_k e^{i2\pi Pk/N_f}$.

We denote the magnitude of the samples, g_k, by h_k. Then

$$h_k = \frac{1}{N_f} \left| \sum_{n=0}^{N_f-1} v_n e^{-i2\pi nk/N_f} \right| \quad . \tag{15}$$

The sequence h_k is called the down-range image sequence. It is seen that this sequence is periodic in k with period N_f. In practice the labor involved in evaluating the h_k is minimized by employing one of a number of versions of the fast Fourier transform (FFT)[3,4] algorithm.

ΔX, which is the generally accepted measure of the down-range resolution of the radar,[1] is referred to as the resolution cell length in this report. Note that the bandwidth, B, of the radar is

$$B \equiv (N_f - 1)\Delta f \quad . \tag{16}$$

[3] A. V. Oppenheim and R. W. Schafer, ***Digital Signal Processing***, *Prentice Hall (1975).*

[4] R. W. Ramirez, ***The FFT Fundamentals and Concepts***, *Prentice Hall (1985).*

[1] R. N. Trebits, ***Synthetic Aperture Radar***, *in* ***Principles of Modern Radar***, *J. L. Eaves and E. K. Reedy, eds, Van Nostrand Reinhold (1987), pp 502–537.*

Therefore if $N_f >> 1$, as is usually the case,

$$\Delta X \equiv \frac{c}{2B} \quad . \tag{17}$$

We see that the down-range interval of high-reflectivity points at X_k which are sampled is

$$X_{N_f-1} - X_0 = (N_f - 1)\,\Delta X \quad .$$

Since it was assumed that the entire target is within a sampling interval, L must satisfy

$$0 < L \leq N_f \Delta X \quad . \tag{18}$$

This condition on L is assumed to be satisfied for all the discussions and images in this report, whether or not the target lies entirely in a single-sampling interval. The sole exception is the single-point reflector, discussed in section 9, for which, strictly speaking, $L = 0$.

The sampling length, R, given in equation (4), may be considered to be the "unambiguous range" of the radar. The significance of this terminology becomes clear from the discussions of section 5.

The "down-range image" is obtained by plotting a histogram consisting of N_f bars, each of whose width is ΔX and whose height is one of the magnitudes, h_k, of the down-range image sequence. Unless stated otherwise, in this report the order in which the bars are plotted on the image histogram in the direction of increasing X is the "normal order" of the k's, i.e.,

$$0, 1, 2, 3, \ldots, N_f - 1 \quad . \tag{19}$$

Then if a bar is plotted as the k^{th} bar, its low-X boundary on the down-range image plot has the down-range coordinate, $k\Delta X$, and its high-X boundary has the down-range coordinate $(k + 1)\Delta X$.

4. Effects of Bandwidth and Δf on Image Quality

Equation (17) shows that one must employ a sufficiently large bandwidth to obtain a small enough ΔX to achieve the quality image desired, and equation (4) shows that Δf must be small enough to achieve the required unambiguous range. With the current state of the art in millimeter-wave systems, a 1.5- to 2-GHz bandwidth can be achieved, which results in a 7.5- to 10-cm resolution. From equation (4) the Δf required for an unambiguous range of 15 m, which is required for some radar imaging applications, is 10 MHz, and this requirement can be easily satisfied.

5. "Good" and "Bad" Images

Equation (15) was seen to give the down-range image of a target assumed to be entirely within a sampling interval whose left boundary is at MR, with M an integer. We call such a target location a "good" location, and we call the image obtained using the normal ordering of the k's (eq (19)) a "good" image. In general, a "good" image displays each part of the target at the correct down-range location relative to that of every other part of the target. If a target lies in two neighboring sampling intervals, its location is called a "bad" location, and the computation of the resulting image, called a "bad" image, is discussed in this section. In general, a "bad" image displays a low-x segment of the target at the high-x end of the image histogram, in its proper down-range order, and displays the remainder of the target at the low-x end of the image histogram, in its proper down-range order. If it is known that the sampling length, R, is at least twice as large as the target length, L, and the reflectivity of the target is much greater than that of the surrounding area, then recognizing an image as "bad" may not be difficult, since in that case the image may consist of intense low-X and high-X portions separated by a weak central portion whose length is greater than L. In this section we prescribe and justify a procedure for transforming a "bad" image to a "good" image. To do this we must first prove two theorems.

THEOREM 1. The down-range image of an isolated target of finite extent that is obtained using the procedure described above has the following property: If the target is translated along the down-range direction by an amount d meters, then the down-range image of the target in the translated position is, in general, *different*, at least in some details, from that in the original position. However, in the special case

$$d = pR + m\Delta X \text{ meters} , \tag{20}$$

where p and m are positive integers and $m < N_f$, the down-range image of the target in the translated position, based on an image sequence h_k', is identical to that of the target in the original position, based on h_k, if the order of k in the latter sequence (i.e., the normal order given in eq (19)) is cyclically permuted to the new order

$$N_f - m,\ N_f - m + 1,\ N_f - m + 2,\ ...,\ N_f - 1, 0, 1, 2, ...,\ N_f - m - 1 . \tag{21}$$

PROOF: When the target is in the translated position, the return signal v_n' at frequency f_n is, from equation (3),

$$\begin{aligned} v_n' &= \int_{x_a+d}^{x_b+d} G(x-d)\, e^{i2\pi f_n 2x/c}\, dx \\ &= e^{i2\pi f_n 2d/c} v_n \quad , \end{aligned} \tag{22}$$

as can be seen by making the change in variable $x' = x - d$.

Then by equation (2)

$$v_n' = e^{i2\pi f_0 2d/c}\, e^{i2\pi n \Delta f 2d/c}\, v_n \quad ,$$

and by equation (14)

$$\begin{aligned} g_k' e^{i2\pi Pk/N_f} &= \frac{e^{-i2\pi PM}}{N_f} \sum_{n=0}^{N_f-1} v_n' e^{-i2\pi nkN_f} \\ &= e^{-i2\pi PM}\, e^{i2\pi f_0 2d/c}\, \frac{1}{N_f} \sum_{n=0}^{N_f-1} v_n\, e^{i2\pi n \Delta f 2d/c}\, e^{-i2\pi nk/N_f} \quad . \end{aligned} \tag{23}$$

Comparing equations (14) and (23) we see that, in general, there is no correlation between the shape of the down-range image based on the g_k and that based on the g_k'. However, if d satisfies the condition of equation (20) then, using equations (4) and (5), and noting that $e^{i2\pi np} = 1$, we find that equation (23) becomes

$$\begin{aligned} g_k' e^{i2\pi Pk/N_f} &= e^{-i2\pi PM}\, e^{i2\pi f_0 2d/c}\, \frac{1}{N_f} \sum_{n=0}^{N_f-1} v_n\, e^{-i2\pi n(k-m)/N_f} \\ &= e^{i2\pi f_0 2d/c}\, g_{k-m}\, e^{i2\pi p(k-m)/N_f} \quad , \end{aligned} \tag{24}$$

the latter following from equation (14).

Since the sequence g_k is periodic in k with period N_f, as was noted above, equation (24) yields the result

$$\begin{aligned} h_k' &= h_{N_f+k-m} \quad , \text{ for } k \le m \quad , \\ h_k' &= h_{k-m} \quad , \qquad \text{for } k \ge m \quad . \end{aligned} \tag{25}$$

From equation (25) one sees that if the h_k are plotted with k ordered as in equation (21), the resulting image is that of the translated target. QED.

In view of Theorem 1, any down-range image of an isolated target at a particular down-range location, obtained by ordering k according to any of the N_f cyclic permutations of the "normal order" given in equation (19), is "equivalent" to any other one, in the sense that it corresponds to another down-range location of the *same* target separated by some distance d from the original location, where d satisifes equation (20). As a special case, if, in equation (20), $m = 0$, so that $d = pR$, equation (25) shows that $h_k' = h_k$ for all k. Thus all translations of the target by an integral number of R meters produce the identical down-range image.

Let the low-x and high-x boundaries of the target be

$$x_a = p_a R + q_a \Delta X \tag{26}$$

and

$$x_b = p_b R + q_b \Delta X \quad , \tag{27}$$

where p_a and p_b are positive integers, and $0 \le q_a < N_f$ and $0 < q_b \le N_f$.

Then, in view of the definition of L and equations (5), (26), and (27), the condition of equation (18) becomes, for all our targets,

$$0 < (p_b - p_a) N_f + (q_b - q_a) \le N_f \quad . \tag{28}$$

Therefore, the location of the target falls into one of two classes: For a "good" location

$$p_b = p_a \text{ and } 0 \le q_a < q_b \le N_f \quad , \tag{29}$$

and for a "bad" location,

$$p_b = p_a + 1 \text{ and } 0 \le q_b < q_a < N_f \quad . \tag{30}$$

THEOREM 2. The target location can be changed from "bad" to "good" by translating the target by $m\Delta X$ meters, where m is any integer in the range

$$N_f - q_a \le m \le N_f - q_b \quad , \tag{31}$$

with the first and second equalities applying when q_a and q_b are integers, respectively.

PROOF: Since the target location is "bad," equations (26), (27), and (30) apply. Now consider translating the target by $m_1 \Delta X$ meters. Denote the translated values of x_a and x_b by x_a' and x_b' respectively. Then equations (26), (30), and (5) give

$$x_a' = (p_a + 1) N_f \Delta X + (m_1 + q_a - N_f) \Delta X \ , \tag{32}$$

where $N_f \Delta X$, has been added and subtracted. Equations (27), (30), and (5) give

$$x_b' = (p_a + 1) N_f \Delta X + (m_1 + q_b) \Delta X \ . \tag{33}$$

Let m_1 be the integer satisfying

$$N_f - q_a \le m_1 < N_f - q_a + 1 \ , \tag{34}$$

with the equality applying when q_a is itself an integer. Thus, m_1 clearly satisfies the first inequality in equation (31). Equation (34) may be written as

$$0 \le m_1 + q_a - N_f < 1 \ . \tag{35}$$

Since $q_a < N_f$ and $0 < q_b$, we have

$$m_1 + q_a - N_f < m_1 + q_b \ . \tag{36}$$

In view of the first inequality of equations (35) and (36), we see from the definition of "good" location in equation (29) that the translation through $m_1 \Delta X$ meters resulting in the location described by equations (32) and (33) has moved the target from a "bad" location to a "good" location. Equations (32) and (35) also show that m_1 is the *smallest* integer that can accomplish this, since the low-x end of the target either coincides with the low-x end of a sampling length or is some distance less than one cell length, ΔX, to the right of that end. Thus the first inequality in equation (31) has been proven.

Equations (26) through (30) show that if a location is "good," the *maximum* amount, $s\Delta X$, with s an integer, through which the target can be translated while still maintaining its location as "good" is such that

$$s \leq N_f - q_b \quad , \tag{37}$$

where the equality applies when q_b is an integer.

Then since equations (32) and (33) describe a "good" location, equations (33) and (37) show that the maximum amount $m_2\Delta X$, with m_2 an integer, through which the target in this "good" location can be translated, while still maintaining the location as "good," is such that

$$m_2 \leq N_f - q_b - m_1 \quad ,$$

or, letting $m = m_1 + m_2$,

$$m \leq N_f - q_b \quad . \tag{38}$$

Thus the second inequality of equation (31) is satisfied. QED.

We see then, from Theorems 1 and 2, that for any target whose extent is less than R in a "bad" location, its resulting "bad" image can be transformed to a "good" one for the *identical target* in some "good" location simply by replotting the measured g_k with the ordering of k cyclically permuted from the normal ordering given in equation (19) by some integer m. The result is that any of the N_f cyclic permutations of the h_k from the "normal" one given in equation (19) may, in principle, correspond to the correct shape of the target. The reason is that, since the target may have any length L less than $N_f\Delta X$, according to Theorems 1 and 2 there are N_f possible combinations of target down-range shape and "good" or "bad" locations that could give rise to the observed down-range image. In practice, however, some prior information about the shape of the target may exist which will limit the number of plausible images. Such may be the case, for example, for a target known to have a length L less than $R/2$ in a low-reflectivity surrounding, as was mentioned in the beginning of this section. The lack of ambiguity as to the location of a point target for $L < R/2$ is demonstrated in section 8. It must be emphasized, however, that in general, the imaging methods discussed in this report do not yield the down-range location and shape of a target unambiguously, even if $L < R$.

6. Point Reflector—General

A model of a real target whose down-range image may be computed in a straightforward numerical manner is a series of N_s point reflectors, each of which has associated with it a positive, real, dimensionless reflectivity ρ_l, and a down-range coordinate, x_l meters, where the index $l = 0, 1, 2, \ldots, N_s - 1$. We will assume, without any loss of generality, that

$$x_m > x_n \quad , \text{ if } m > n \ ; \tag{39}$$

that is, the point reflectors are ordered according to increasing down-range coordinate. In this case the integral for v_n in equation (3) becomes a sum over all the reflectors:

$$v_n = \sum_{l=0}^{N_s-1} \rho_l \, e^{i4\pi f_n x_l/c} \quad , \tag{40}$$

assuming no multiple reflections, with the frequency, f_n, given in equation (2).

Let d_l be the location of the l^{th} particle relative to X_0, that is,

$$x_l = X_0 + d_l \ . \tag{41}$$

Then, using equations (2), (6), (12), and (41) in equation (40), the result is

$$v_n = e^{i2\pi PM} \sum_{l=0}^{N_s-1} \rho_l \, e^{i2\pi(P+n)\,\Delta f 2d_l/c} \ . \tag{42}$$

Using the above expression for v_n in equation (15) and reversing the order of summation over n (frequencies) and l (point reflectors) yields

$$g_k = \frac{1}{N_f} \sum_{l=0}^{N_s-1} \rho_l \, e^{i2\pi P \Delta f 2d_l/c} \sum_{n=0}^{N_f-1} \exp\left[-i2\pi n\left(\frac{k}{N_f} - \frac{\Delta f 2d_l}{c}\right)\right] \ . \tag{43}$$

The summation over n in equation (43) is that of a geometric series:

$$\sum_{n=0}^{N-1} e^{ian} = \frac{e^{iaN/2}}{e^{ia/2}} \, \frac{\sin(aN/2)}{\sin(a/2)} \ .$$

Therefore, using equations (4) and (5), the general result for the down-range image of a point reflector target is

$$h_k = \frac{1}{N_f} \left| \sum_{l=0}^{N_s-1} \rho_l e^{i2\pi P d_l / R} \frac{\exp\left[\frac{i\pi d_l}{\Delta X}\right]}{\exp\left[-i\frac{\pi}{N_f}\left(k - \frac{d_l}{\Delta X}\right)\right]} \frac{\sin\left(\frac{\pi d_l}{\Delta X}\right)}{\sin\left[\frac{\pi}{N_f}\left(k - \frac{d_l}{\Delta X}\right)\right]} \right| . \quad (44)$$

7. Explanation of Figures

Each of the figures in the report is one of a set of images of a point reflector illustrating some property to be discussed in the following sections. In each of these figures, Δf = 10 MHz and N_f = 64. Using $c = 3 \times 10^8$ m/s yields R = 15 m and ΔX = 15/64 m = 0.234 m. Each of the 13 down-range axis major divisions represents a length $5\Delta X$ = 1.170 m. The latter are further subdivided into five minor divisions, each of length ΔX. Thus the total length of the down-range axis is $65\Delta X$. For all the point targets in the figures, the low-x coordinate, x_a, is between $6R$ and $7R$. Therefore, the absolute range covered by the image is 90 to 105 m. As indicated in the x-axis label of the histograms, down-range distance is plotted in units of ΔX, beginning at 90 m from the radar ($6R$).

Having been given the values of ρ_l and x_l for each target point, we calculate the return signals, v_n, from equation (40) and the image histogram from equation (15). Each ρ_l is given as some multiple of a reflectivity ρ. Therefore, as equations (40) and (15) show, each h_k will, in turn, be proportional to ρ. In each case the values calculated for the h_k were normalized, so that the height of the histogram bar representing the maximum value of h_k was assigned the entire extent of the amplitude axis, i.e., 10 major divisions. If we denote the maximum value of h_k by $y_{max}\rho$, then the normalization factor is $y_{max}\rho/10$. This factor is indicated in the y-axis label in each histogram.

The down-range locations of each point of the target are indicated by a dot plotted on the down-range axis and labelled with the corresponding value of l. In addition, the values of ρ for each target point and its down-range location, both in meters and in the form $6R + q\Delta X$, are stated in the figure. In figures 1d and 2d the value of q for target point 2 is greater than 65 (i.e., the down-range location of this point is off the scale). This is indicated in those figures by target point 2 being plotted on a broken extension to the down-range axis.

Included in each set of figures that illustrates some property is a table giving the placement of the points and peaks of the down-range image; this alternative form is provided for the convenience of the reader. The symbols in the column headings refer to lowest radar frequency (f_0), down-range location of point-reflector 0 (x_0), down-range location of center of

resolution cell in which point reflector 0 is imaged less x_0 (Δx_0), the same for point reflectors 1 and 2 (x_1, Δx_1, x_2, Δx_2), reflectivity of point reflector 0 in units of ρ (ρ_0/ρ), peak amplitude in the image for point reflector 0 in units of ρ (y_0/ρ), and the same for point reflectors 1 and 2 (ρ_1/ρ, y_1/ρ, ρ_2/ρ, y_2/ρ).

8. Translating Point Reflector Targets

Theorem 1 in section 4, which was proven for any target, can be seen to be true for a point target merely by inspection of equation (44). Thus if the target is translated by an amount d, so that d_l becomes $d_l' = d_l + d$, equation (44) becomes

$$h_k' = \frac{1}{N_f} \left| \sum_{l=0}^{N_s-1} \rho_l e^{i2\pi d_l/R} \frac{\exp\left[\frac{i\pi d_l}{\Delta X}\right]}{\exp\left[-i\,\frac{\pi}{N_f}\left(k - \frac{d_l}{\Delta X}\right)\right]} \frac{\sin\left[\pi\left(\frac{d_l}{\Delta X} + \frac{d}{\Delta X}\right)\right]}{\sin\left[\frac{\pi}{N_f}\left(k - \frac{d_l}{\Delta X}\right)\right]} \right| . \quad (45)$$

So, in general, there is no correlation between h_k' and h_k. However, if d satisfies the condition of equation (20), evaluating equation (45) with such a value of d yields the relation between h_k' and h_k in equation (25).

Figures 1 and 2 illustrate the effects on the image of translating a point reflector target by amounts d that do not and do satisfy equation (20), respectively. The target in these figures consists of three points with $\rho_0 = 2\rho$, $\rho_1 = \rho$, and $\rho_2 = 2\rho$. The spacings of the points are $x_1 - x_0 = 2$ m and $x_2 - x_1 = 3$ m. The lowest radar frequency, f_0, is 95 GHz. For figures 1a and 2a, which are identical to each other, $x_a = x_0 = 90$ m $= 6R$. For figure 1b, $x_a = x_0 = 95$ m, so that the translation, d, of the target relative to its position in figure 1a is 5 m, which does not satisfy equation (20). Therefore not only is the image in figure 1b translated relative to that of figure 1a, but even its shape (that is, the relative magnitudes of the histogram bars) is different. For figure 2b, however, the translation relative to the target location of figure 2a is $22\Delta X$ exactly. Hence in this case d satisfies equation (20) ($p = 0$, $m = 22$), and, thus, the image in figure 2b is translated relative to that of figure 2a, but the shapes of the two are identical.

The parameters p_a, p_b, q_a, and q_b for the end-point locations of a target have been defined in equations (26) and (27), and the criteria for "good" and "bad" locations were given in equations (29) and (30), respectively. These parameters for figures 1 and 2 are given in table 1. Since figures 1a,

2b, point reflectors 0 and 1 are imaged at approximately the correct location, but point reflector 2 is imaged at 90 m instead of at 105 m. In figures 1d and 2c, point reflector 0 is imaged at approximately the correct location, but point reflectors 1 and 2 are imaged at about 90 and 95 m, respectively, instead of at 105 and 108 m, respectively.

Figure 1. Dependence of shape of down-range image of a point target on target locations separated by non-integral multiples of a sampling cell length: f_0 = 95 GHz, R = 15 m, ΔX = 0.234 m, $\rho_0 = 2\rho$, $\rho_1 = \rho$, $\rho_2 = 2\rho$.

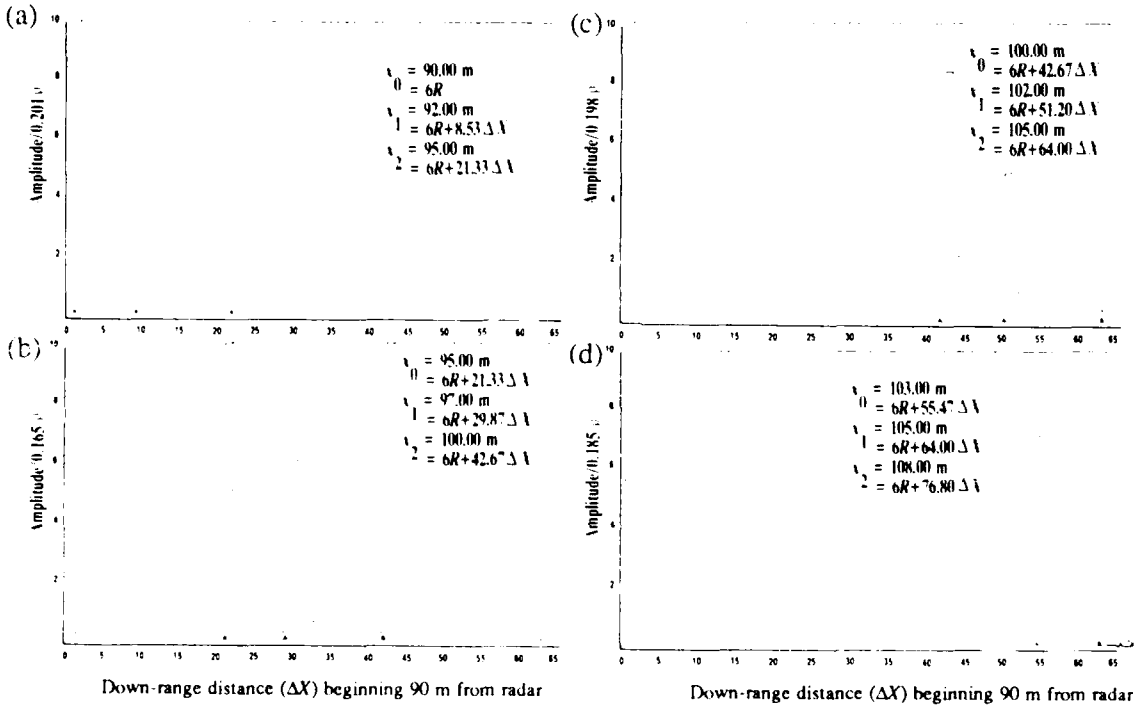

Fig.	f_0 (GHz)	x_0 (m)	Δx_0 (m)	x_1 (m)	Δx_1 (m)	x_2 (m)	Δx_2 (m)	$\frac{\rho_0}{\rho}$	$\frac{y_0}{\rho}$	$\frac{\rho_1}{\rho}$	$\frac{y_1}{\rho}$	$\frac{\rho_2}{\rho}$	$\frac{y_2}{\rho}$
1a	95	90.0	0.0	92.0	0.2	95.0	0.0	2.0	2.0	1.0	0.7	2.0	1.6
1b	95	95.0	0.0	97.0	0.1	100.0	0.2	2.0	2.0	1.0	1.2	2.0	2.0
1c	95	100.0	0.2	102.0	0.1	105.0	−14.9	2.0	1.7	1.0	1.0	2.0	2.0
1d	95	103.0	0.0	105.0	−14.9	108.0	−14.8	2.0	1.3	1.0	1.0	2.0	1.9

Figure 2. Invariance of shape of down-range image of a point target with target locations separated by integral multiples of a sampling cell length: f_0 = 9.5 GHz, R = 15 m, ΔX = 0.234 m, $\rho_0 = 2\rho$, $\rho_1 = \rho$, $\rho_2 = 2\rho$.

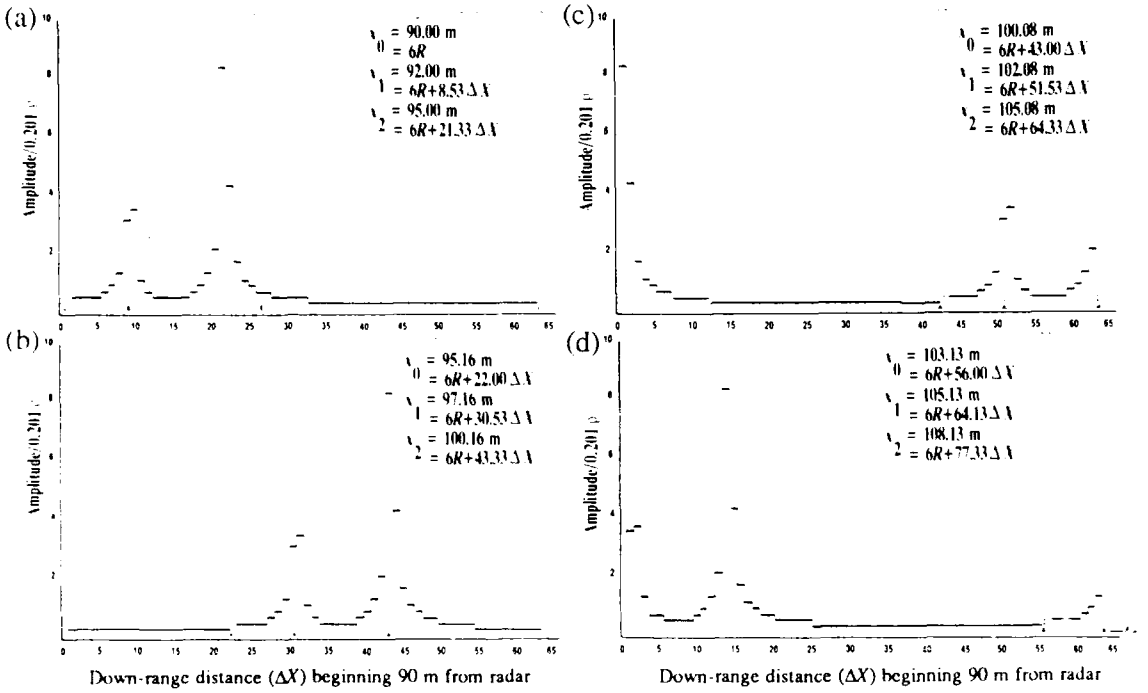

Fig.	f_0 (GHz)	x_0 (m)	Δx_0 (m)	x_1 (m)	Δx_1 (m)	x_2 (m)	Δx_2 (m)	$\frac{\rho_0}{\rho}$	$\frac{y_0}{\rho}$	$\frac{\rho_1}{\rho}$	$\frac{y_1}{\rho}$	$\frac{\rho_2}{\rho}$	$\frac{y_2}{\rho}$
2a	95	90.0	0.0	92.0	0.2	95.0	0.0	2.0	2.0	1.0	0.7	2.0	1.6
2b	95	95.2	0.1	97.2	0.2	100.2	0.0	2.0	2.0	1.0	0.7	2.0	1.6
2c	95	100.1	0.1	102.1	10.2	105.1	−15.0	2.0	2.0	1.0	0.7	2.0	1.6
2d	95	103.1	0.1	105.1	−15.0	108.1	−14.9	2.0	2.0	1.0	0.7	2.0	1.6

Despite the fact that point reflector 2 in figure 2c and point reflectors 1 and 2 in figure 2d are imaged at incorrect down-range locations because of the "bad" location of the target, the shapes of the images of each of those point reflectors are identical to the shapes of the images of the corresponding point reflectors in figures 2a and 2b. The reason is that, just as for figure 2b, figures 2c and 2d are brought about by translations which satisfy equation (20), i.e., $d = 43\Delta X$ and $d = 56\Delta X$ for figures 2c and 2d, respectively. By contrast, not only do the images in figures 1c and 1d display those point reflectors at incorrect down-range locations because of the "bad" location of the target, but the shapes of the images of individual point reflectors are different from those of corresponding individual point reflectors in figure 1a. The reason is that, just as for figure 1b, the target locations of figures 1c and 1d are brought about by translations which do not satisfy equation (20).

Equation (31) gives the range of the integral number of ΔX through which a target in a "bad" location could be translated to convert its location to a "good" one. Using the data in the table of figure 1 in this equation, one finds that the range of translations from the target location of figure 2d which accomplishes this is $8\Delta X$ through $50\Delta X$. If a translation through $8\Delta X$ is performed, we see from the table that q_a and q_b would become 0.000 and 21.333, respectively, which is the same as the values for figure 2a, in which point reflector 0 is imaged at the extreme left of the histogram. However, now the values of p_a and p_b would be 7 instead of 6. If a translation through $50\Delta X$ is performed, we see from the table that q_a and q_b would become 42.000 and 63.333, and again $p_a = p_b = 7$. This would result in the "good" image for which point reflector 2 is imaged as far to the right as possible with shapes of the images of individual point reflectors identical to those of figure 2a.

Table 1. "Good" and "bad" location parameters for point targets: R = 15 m, ΔX = 15/64 m = 0.234 m

Fig.	x_a (m)	x_b (m)	p_a	p_b	q_a	q_b	Location type
1a	90.000	95.000	6	6	0.000	21.333	"good"
1b	95.000	100.000	6	6	21.333	42.667	"good"
1c	100.000	105.000	6	7	42.667	0.000	"bad"
1d	103.000	108.000	6	7	55.467	12.800	"bad"
2a	90.000	95.000	6	6	0.000	21.333	"good"
2b	95.156	100.156	6	6	22.000	43.333	"good"
2c	100.078	105.078	6	7	43.000	0.333	"bad"
2d	103.125	108.078	6	7	56.000	13.333	"bad"

The smallest integer number of ΔX through which the target of figure 2d would have to be translated to correct its image to a "good" one was determined above to be 8. This determination was made using equation (31) and our knowledge of the precise location of the target. However, if one knew only that the length of the target is less than $R/2$ = 7.5 m and the reflectivity of the surrounding area is zero, one would know by inspection that the image of figure 2d was "bad," since there is a 10-m gap between the first and second peaks of the image. Then, by simple inspection of the histogram, one would determine that the smallest integer m by which the h_k would have to be cyclically permuted from their "normal" order (eq (19)) to produce the "good" image of figure 2a is 8. Thus, the target location may be determined unambiguously in this case. However, as mentioned in section 5, the imaging methods described here do not, in general, allow one to determine target location, and, correspondingly, target shape, unambiguously.

9. Target Consisting of a Single Point Reflector

The simplest point-reflector target is that containing a single point reflector. Assume that the point reflector has radar reflectivity, ρ, and is located at a down-range position of $X_0 + d$. Then equation (44) becomes, for this case,

$$h_k = \left| \frac{\rho \sin\frac{\pi d}{\Delta X}}{N_f \sin\left[\frac{\pi}{N_f}\left(k - \frac{d}{\Delta X}\right)\right]} \right| . \tag{46}$$

If the point is located precisely at the left edge of the l^{th} down-range resolution cell, that is, $d = l\Delta X$ with l an integer less than N_f, then equation (46) yields the result

$$\begin{aligned} h_k &= \rho \ , \ \text{for } k = l \ , \\ h_k &= 0 \ , \ \text{otherwise} \ . \end{aligned} \tag{47}$$

This, of course, is the expected result, since then the sampling procedure for the actual target function, $G(X)$, discussed in section 2, is exact.

If the point is inside the l^{th} down-range resolution cell, equation (46) will yield a value for h_l that is less than ρ, and values for h_k with k-values near l that are nonzero.

Table 2 gives values of h_k/ρ for $N_f = 64$ for the point located at the left edge of the l^{th} cell as well as one-quarter, one-half, and three-quarters of the way into the l^{th} cell. The histogram images for these cases are in figures 3a through 3d, respectively. The lowest radar frequency, f_0, is again 95 GHz.

Table 2. Single point at $X_0 + d$ for $N_f = 64$

$\frac{d}{\Delta X} - l$	$\frac{h_{l-2}}{\rho}$	$\frac{h_{l-1}}{\rho}$	$\frac{h_l}{\rho}$	$\frac{h_{l+1}}{\rho}$	$\frac{h_{l+2}}{\rho}$
0	0	0	1	0	0
1/4	0.100	0.180	0.900	0.300	0.129
1/2	0.128	0.212	0.637	0.637	0.212
3/4	0.082	0.129	0.300	0.900	0.180

We note that when the point reflector is half-way through the l^{th} cell, the distribution has a peak of width $2\Delta X$, with equal peak values in both the l^{th} and $(l+1)^{th}$ cells. This occurs because in this case the point is equidistant from the left edge of both those cells. When the point is three-quarters of the way through the l^{th} cell, the distribution peaks in the $(l+1)^{th}$ cell, since the point is closer to the left edge of the $(l+1)^{th}$ cell than to that of the l^{th} cell. In this case, basing the determination of the point's location simply on the cell which has the maximum distribution would give an erroneous result.

Figure 3. Dependence of shape of down-range image of a single-point on location of point within a sampling cell: $f_0 = 95$ GHz, $R = 15$ m, $\Delta X = 0.234$ m, $\rho_0 = \rho$.

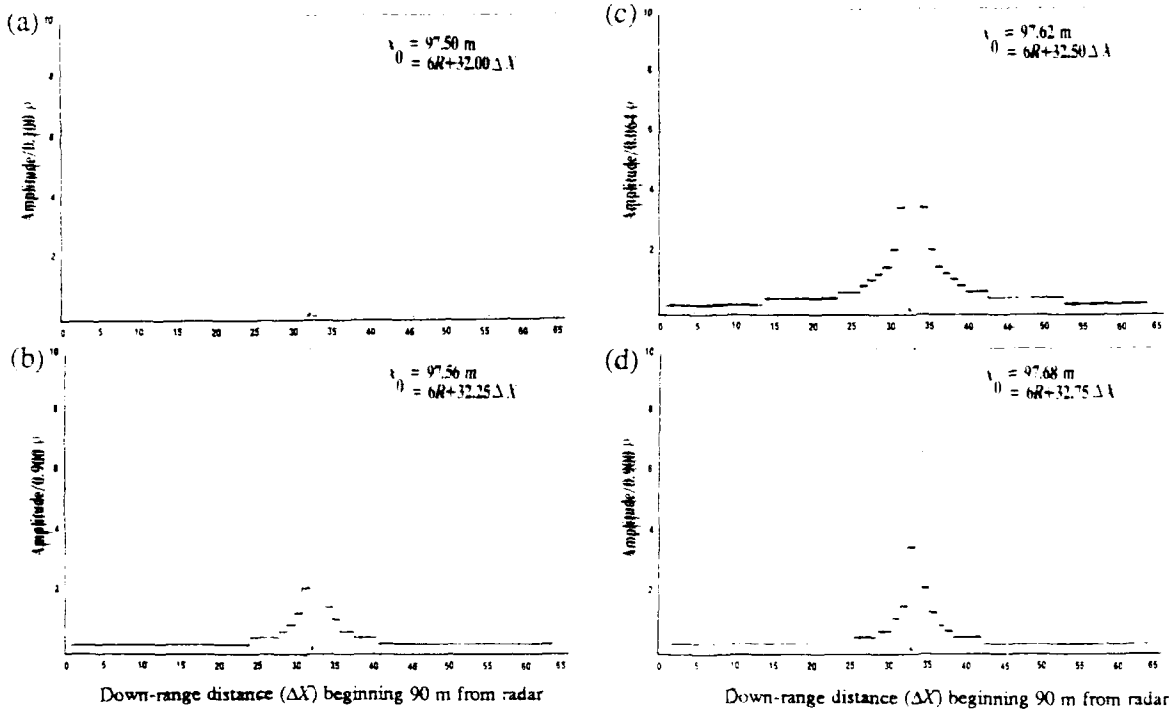

Fig.	f_0 (GHz)	x_0 (m)	Δx_0 (m)	$\frac{\rho_0}{\rho}$	$\frac{y_0}{\rho}$
3a	95	97.5	0.0	1.0	1.0
3b	95	97.6	–0.1	1.0	0.9
3c	95	97.6	0.0	1.0	0.6
3d	95	97.7	0.2	1.0	0.9

10. Target Consisting of Equally Spaced Point Reflectors

If the point reflectors have equal spacing d, so that

$$d_l = d_0 + ld \quad , \quad l = 0, 1, 2, ..., N_s - 1 \quad ,$$

equation (44) becomes

$$h_k = \frac{1}{N_f} \left| \sum_{l=0}^{N_s-1} \rho_l e^{i2\pi Pld/r} \frac{\exp\left[\frac{i\pi ld}{\Delta X}\right]}{\exp\left[-i\frac{\pi}{N_f}\left(k - \frac{ld}{\Delta X}\right)\right]} \frac{\sin\left[\pi\left(\frac{d_0}{\Delta X} + \frac{ld}{\Delta X}\right)\right]}{\sin\left[\frac{\pi}{N_f}\left(k - \frac{d_0}{\Delta X} - \frac{ld}{\Delta X}\right)\right]} \right| \tag{48}$$

If $d_0 = K\Delta X$ and $d = N\Delta X$, with K and N integers (i.e., all reflectors are on an edge of a down-range resolution cell), then $N_s \leq N_f$, and equation (48) gives

$$\begin{aligned} h_k &= \rho_k \quad , \text{ for } k = k + N_l \quad , \\ h_k &= 0 \quad , \text{ otherwise} \quad . \end{aligned} \tag{49}$$

This again is the expected result based on the discussion in section 2.

In general, the shape of the image histogram calculated from equation (48) for a given N_f, Δf, d, and reflectivities ρ_l depends on the ratio $P = f_0/\Delta f$. However, consider two values of f_0, f_a and f_b, having ratios to Δf, P_a and P_b, such that

$$P_b = P_a + \frac{pR}{d} \quad , \tag{50}$$

where p is an integer. Then, since $e^{i2\pi pl} = 1$, equation (48) gives the same result for f_a and f_b. Therefore the images for these two frequencies will be identical in shape. From equation (50), f_a and f_b are related by

$$f_b = P_b \Delta f = f_a + p\,\frac{c}{2d} \quad . \tag{51}$$

Thus, for example, if d = 1 m, $c/2d$ = 1.5 GHz. Then one would expect the shapes of the images at 1.0 and 10.0 GHz to be the same, at 1.5 and 10.5 GHz to be the same, and at 35 and 95 GHz to be the same. That this is so is illustrated in figures 4a, 4b, and 4c, respectively, for a target consisting of three points with reflectivities ρ, 2ρ, and 3ρ, located 95, 96, and 97 m down range. The shape for any one of these pairs of frequencies, however, would be expected to differ from the shape for any of the other two pairs. Therefore, there are detailed differences in the shapes of the histograms of figures 4a, 4b, and 4c.

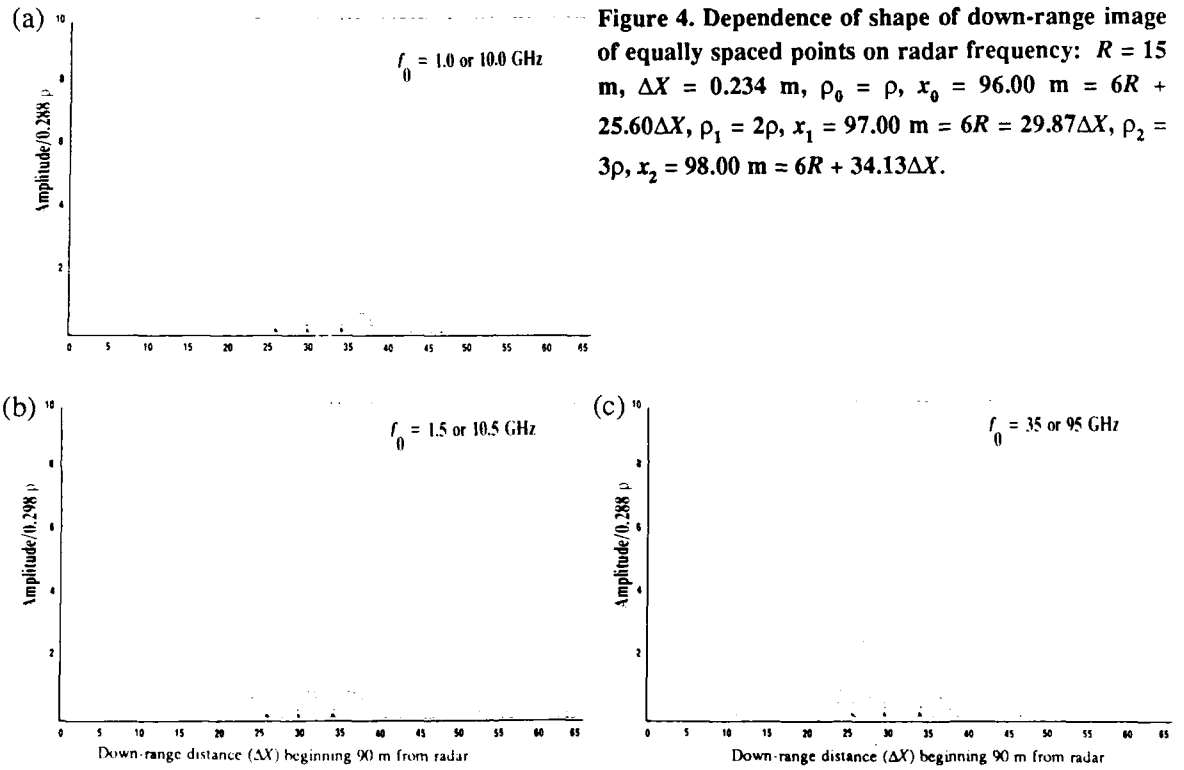

Figure 4. Dependence of shape of down-range image of equally spaced points on radar frequency: R = 15 m, ΔX = 0.234 m, $\rho_0 = \rho$, x_0 = 96.00 m = $6R$ + $25.60\Delta X$, $\rho_1 = 2\rho$, x_1 = 97.00 m = $6R$ = $29.87\Delta X$, $\rho_2 = 3\rho$, x_2 = 98.00 m = $6R$ + $34.13\Delta X$.

Fig.	f_0 (GHz)	x_0 (m)	Δx_0 (m)	x_1 (m)	Δx_1 (m)	x_2 (m)	Δx_2 (m)	$\frac{\rho_0}{\rho}$	$\frac{y_0}{\rho}$	$\frac{\rho_1}{\rho}$	$\frac{y_1}{\rho}$	$\frac{\rho_2}{\rho}$	$\frac{y_2}{\rho}$
4a	1.0; 10.0	96.0	0.2	97.0	0.1	98.0	0.1	1.0	0.7	2.0	2.0	3.0	2.9
4b	1.5; 10.5	96.0	0.2	97.0	0.1	98.0	0.1	1.0	0.7	2.0	2.1	3.0	3.0
4c	35; 95	96.0	0.2	97.0	0.1	98.0	0.1	1.0	0.9	2.0	1.8	3.0	2.9

11. Deducing Relative Point Locations and Cross Sections from Images

It should be noted that despite the difference in the detailed shapes of the histograms in figure 4, all of them can be quite unambiguously interpreted as representing the image of three points separated by $4\Delta X \cong 1$ m. It is also clear from all of them that $\rho_0 < \rho_1 < \rho_2$. However, it is seen that the ratio of the peak heights is not necessarily a reliable measurement of $\rho_0 : \rho_1 : \rho_2$. These ratios are 1.0 : 2.8 : 4.2 for figure 4a, 1.0 : 2.9 : 4.2 for figure 4b, and 1.0 : 2.1 : 3.3 for figure 4c. Since the correct ratio is 1 : 2 : 3, the set of "measurements" at 35 and 95 GHz seems to have yielded the most accurate ratio in this case. However, figure 5 illustrates the fact that the ratio of image heights of point reflectors of given reflecivity is quite sensitive to the exact location of the point target. In figure 5, f_0 = 95 GHz and the target is the same as in figure 4; x_0 is 96 m in figure 5a, 96 + $\Delta X/4$ m in figure 5b, 96 + $\Delta X/2$ m in figure 5c, and 96 + $3\Delta X/4$ m in figure 5d. The peak height ratios in these figures are

1.0 : 2.1 : 3.3,
1.0 : 1.7 : 4.8,
1.0 : 1.5 : 2.4, and
1.0 : 2.2 : 3.8,

respectively.

Figure 5. Dependence of ratios of peak heights in down-range image of points of different reflectivity on location of points relative to a sampling cell edge: f_0 = 95 GHz, R = 15 m, ΔX = 0.234 m, $\rho_0 = \rho$, $\rho_1 = 2\rho$, $\rho_2 = 3\rho$.

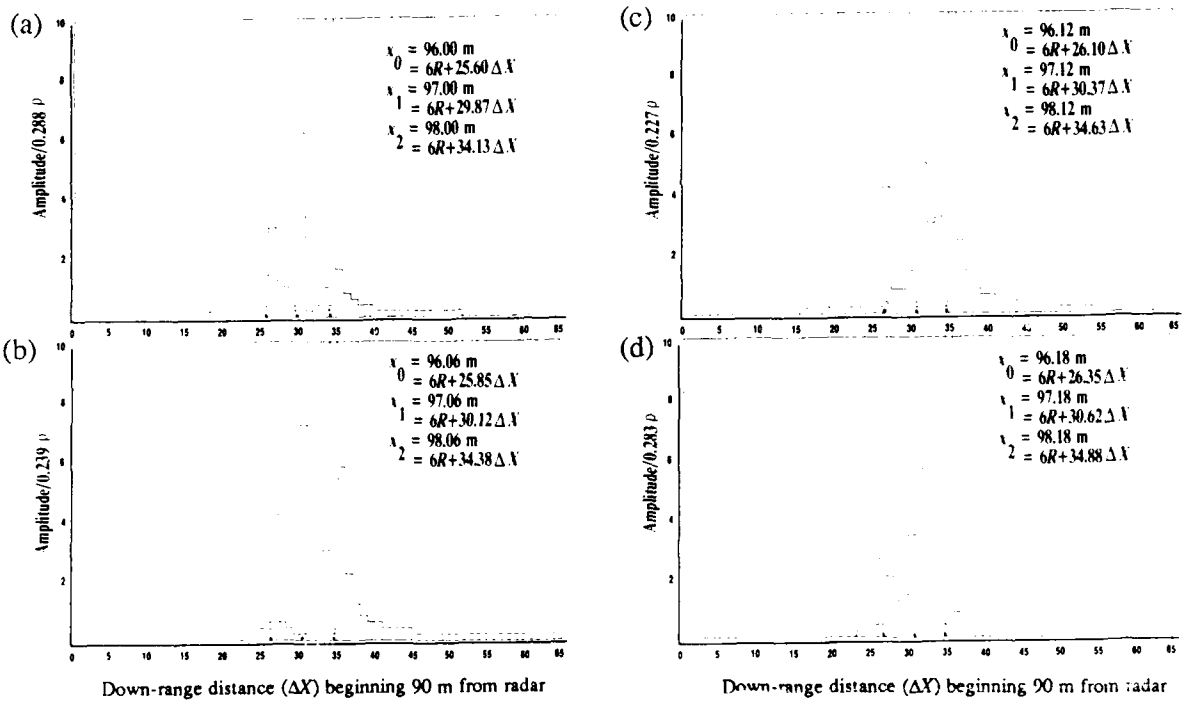

Fig.	f_0 (GHz)	x_0 (m)	Δx_0 (m)	x_1 (m)	Δx_1 (m)	x_2 (m)	Δx_2 (m)	$\frac{\rho_0}{\rho}$	$\frac{y_0}{\rho}$	$\frac{\rho_1}{\rho}$	$\frac{y_1}{\rho}$	$\frac{\rho_2}{\rho}$	$\frac{y_2}{\rho}$
5a	95	96.0	0.0	97.0	0.1	98.0	0.1	1.0	0.9	2.0	1.8	3.0	2.9
5b	95	96.1	0.1	97.1	0.0	98.1	0.0	1.0	1.0	2.0	1.7	3.0	2.4
5c	95	96.1	0.1	97.1	0.0	98.1	0.2	1.0	1.0	2.0	1.5	3.0	2.3
5d	95	96.2	0.0	97.2	−0.1	98.2	0.1	1.0	0.7	2.0	1.6	3.0	2.8

12. Properties of the h_k^2

It was seen in equation (15) that the image samples, h_k, are proportional to the DFT of the field strength ratios, v_n. Therefore, from Parseval's relation for the DFT,[3]

$$\sum_{k=0}^{N_f-1} h_k^2 = \frac{1}{N_f} \sum_{n=0}^{N_f-1} |v_n|^2 \tag{52}$$

where $|v_n|$ is the magnitude of v_n.

From the general expression for the v_n for point reflectors, equation (40), one then obtains the result

$$\sum_{k=0}^{N_f-1} h_k^2 = \sum_{l=0}^{N_s-1} \rho_l^2 + \frac{2}{N_f} \sum_{\substack{l=0 \\ l<m}}^{N_s-1} \sum_{m=0}^{N_s-1} \rho_l \rho_m \cos\left[\pi(\alpha_{lm})\left(1 - \frac{1}{N_f} + \frac{2P}{N_f}\right)\right] \frac{\sin(\pi\alpha_{lm})}{\sin\left(\frac{\pi\alpha_{lm}}{N_f}\right)} \tag{53}$$

where

$$\alpha_{lm} = \frac{x_l - x_m}{\Delta X} \quad , \tag{54}$$

and the double sum extends over all pairs of l and m for which $l < m$. It is immediately obvious from equation (46) that if the point reflectors are all separated by an integer times a sampling cell length, ΔX, then

$$\sum_{k=0}^{N_f-1} h_k^2 = \sum_{l=0}^{N_s-1} \rho_l^2 \quad . \tag{55}$$

Thus, in this case the point reflectors are completely "decoupled" from each other.

It was shown in section 10 that if each point reflector is located on a boundary of a resolution cell,

$$h_k = \rho_k \quad ,$$

when k corresponds to one of the point locations, and

$$h_k = 0 \quad ,$$

otherwise. Therefore equation (55) is exactly satisfied for such a case.

[3] *A. V. Oppenheim and R. W. Schafer, **Digital Signal Processing**, Prentice Hall (1975).*

Even if the points are not exactly located on resolution cell boundaries, but each point reflector is separated from its nearest neighbor(s) by a large enough number of cell lengths, ΔX, then depending on P and the relative values of the ρ_l, the terms in the double sum of equation (53) will nearly cancel each other, so that equation (55) is approximately true. In such cases the point reflectors are "nearly decoupled" from each other. In these cases the "subsets" of the relationship in equation (55) for each of the point reflectors may also be approximately valid. That is, let k_1 and k_2 be the labels of sample cell boundaries that bracket the point reflector location, x_l, on the left and on the right, respectively. Furthermore, let the separation between the k_1 boundary and x_l, as well as that between x_l and the k_2 boundary, be smaller than the separations between the point reflector and its left and right nearest neighbor points, respectively. Then the partial sum, S_l, is approximately ρ_l^2. That is,

$$S_l \equiv \sum_{k=k_1}^{k_2} h_k^2 = \rho_l^2 \tag{56}$$

is approximately satisfied.

In general, values of h_k for cell boundaries that are far from any point reflector are small compared to those near a point reflector. This is seen to be the case for all the image histograms in figures 1 through 5. Therefore, if equation (56) is approximately satisfied for each of the point reflectors, then equation (55) is also approximately satisfied.

Table 3 shows the extent to which equations (55) and (56) are valid for the point reflector targets of figures 2b and 5a. For figure 2b, the number of terms included in the partial sums was 8, and for figure 5a, it was 4. The relationships in equations (55) and (56) are seen to be true to a better approximation for figure 2b than for figure 5a. The most important difference between the two cases contributing to this result is that the points in the target of figure 2b have about twice as large a separation as those of figure 5a.

Table 3. Test of properties of h_k^2

Fig.	$\frac{\rho_0^2}{\rho^2}$	$\frac{S_0}{\rho^2}$	$\frac{\rho_1^2}{\rho^2}$	$\frac{S_1}{\rho^2}$	$\frac{\rho_2^2}{\rho}$	$\frac{S_2}{\rho^2}$	$\sum_0^2 \frac{\rho_l^2}{\rho^2}$	$\sum_0^{6} \frac{h_k^2}{\rho^2}$
2b	4	4.072	1	0.896	4	3.844	9	8.957
5a	1	1.042	4	3.487	9	8.642	14	13.300

13. Down-Range Resolution for Point Reflectors

Since the sampling cell or down-range resolution is ΔX, one would expect that the images of two points that are separated by a distance ΔX or less will have too large an overlap to allow them to be distinguished. One would, however, expect them to be distinguishable if their separation were larger, say $1.5\Delta X$ or $2.0\Delta X$. Figures 6, 7, and 8 show images of two points, both having reflectivity, ρ, separated by ΔX, $1.5\Delta X$, and $2.0\Delta X$, respectively. In all these figures $f_0 = 95$ GHz.

In figure 6a, $x_a = 6R + 32\Delta X = 97.5$ m. Since the separation of the two point-reflectors is ΔX, the image of figure 6a has the shape described by equation (49) with $N_s = 2$, $K = 32$, $N = 1$, $\rho_0 = \rho_1 = \rho$, and $\rho_k = 0$ for all other k-values. This results in h-values of 1 for the $k = 32$ and $k = 33$ cells of the image. For figures 6b and 6c, the target was translated by $\Delta X/4$ and $\Delta X/2$, respectively, from its position in figure 6a. Therefore, for these cases, the more general expression for h_k in equation (48) must be used. It is seen that no matter how the two points bracket the boundary between the $k = 32$ and $k = 33$ cells, the image will always consist of a single peak with shoulders. Thus the images of the points always overlap to an extent, making them indistinguishable. Translating the target further to the right in steps of $\Delta X/4$ yields images that are correspondingly translated and that have shapes that are either identical to or are mirror images of those for translations up to $\Delta X/2$.

In figure 7a, x_a is again 97.5 m. In contrast to figure 6a, in this case the image consists of a peak in the $k = 32$ cell and a two-cell-wide shoulder in the $k = 33$ and $k = 34$ cells. Thus the two points cannot be distinguished at this position. However, as shown in figure 7b, translating the target slightly by $0.01\Delta X$ allows the two points to be distinguished to some extent. However, the image of reflector 1 appears in the $k = 34$ cell, since this point is now closer to the left edge of that cell than to the left edge of the $k = 33$ cell. As the target is translated further to the right, the two points become more distinguishable, until, with a total translation of $\Delta X/4$, the value in figure 7c, the image consists of two equally intense peaks in the $k = 32$ and $k = 34$ cells. Further translations to the right beyond $\Delta X/4$ give rise to image shapes that are either identical to or are mirror images of those for translations up to $\Delta X/4$.

Figure 6. Dependence of down-range image resolution of two points of equal reflectivity separated by one sampling cell length on location of points relative to a sampling cell edge: f_0 = 95 GHz, R = 15 m, ΔX = 0.234 m, $\rho_0 = \rho_1 = \rho$.

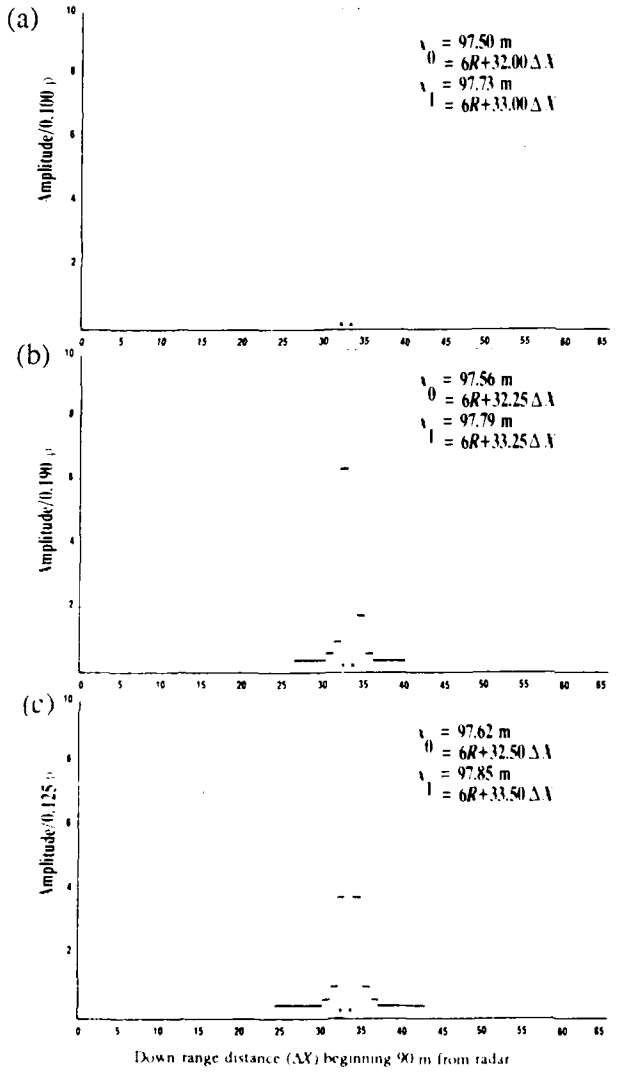

Fig.	f_0 (GHz)	x_0 (m)	Δx_0 (m)	x_1 (m)	Δx_1 (m)	$\frac{\rho_0}{\rho}$	$\frac{y_0}{\rho}$	$\frac{\rho_1}{\rho}$	$\frac{y_1}{\rho}$
6a	95	97.5	*	97.7	*	1.0	*	1.0	*
6b	95	97.6	*	97.8	*	1.0	*	1.0	*
6c	95	97.6	*	97.9	*	1.0	*	1.0	*

**Point not resolved from a neighboring point in image.*

Figure 7. Dependence of down-range image resolution of two points of equal reflectivity separated by 1.5 sampling cell lengths on location of points relative to a sampling cell edge: f_0 = 95 GHz, R = 15 m, ΔX = 0.234 m, $\rho_0 = \rho_1 = \rho$.

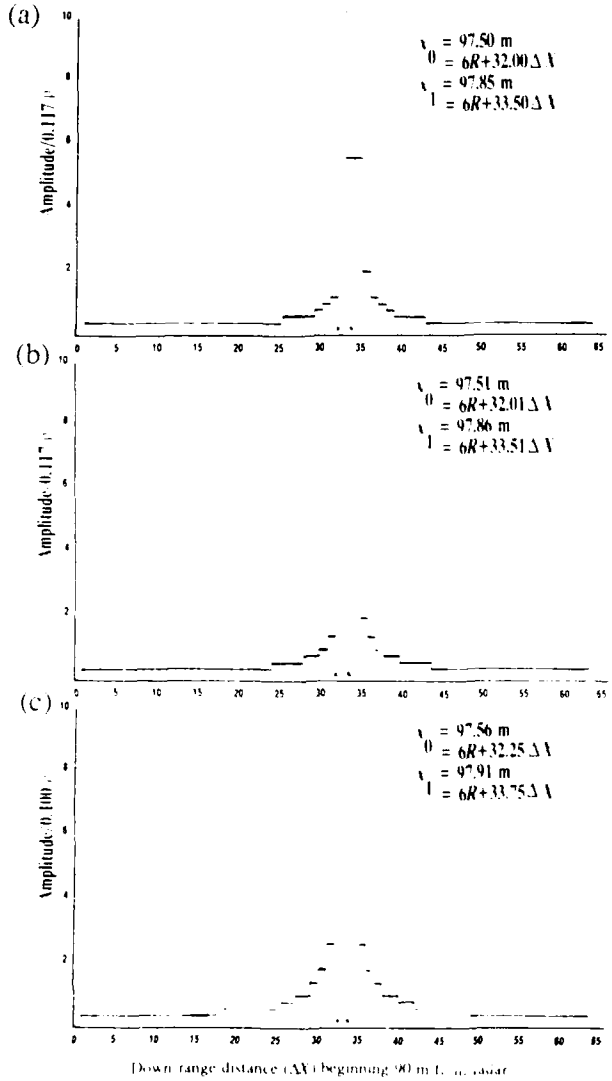

Fig.	f_0 (GHZ)	x_0 (m)	Δx_0 (m)	x_1 (m)	Δx_1 (m)	$\frac{\rho_0}{\rho}$	$\frac{y_0}{\rho}$	$\frac{\rho_1}{\rho}$	$\frac{y_1}{\rho}$
7a	95	97.5	*	97.9	*	1.0	*	1.0	*
7b	95	97.5	0.1	97.9	0.2	1.0	1.2	1.0	0.7
7c	95	97.6	0.0	97.9	0.2	1.0	1.0	1.0	1.0

**Point not resolved from a neighboring point in image.*

For figure 8a, $x_a = 6R + 31\Delta X = 97.266$ m. Since here the separation is $2\Delta X$, rather than ΔX, the proper application of equation (49) is with $N_s = 2$, $K = 31$, $N = 2$, $\rho_{31} = \rho_{33} = \rho$, and $\rho_k = 0$ for all other k-values. This results in h-values of 1 for the $k = 31$ and $k = 33$ cells, which is the shape of the image in this figure. The two points are thus readily distinguishable. In figures 8b through 8k the target is translated by some fraction of ΔX from its position in figure 8a, so that the more general expression for h_k in equation (48) must be used. As the target is translated by small fractions of ΔX the peaks in the $k = 31$ and $k = 33$ cells become less intense, with the intensity in the latter cell decreasing faster than that in the former cell, and shoulders develop, as in figure 8b. As the translation continues, the high-range shoulder of the $k = 33$ cell increases, as in figure 8c, until, in figure 8d, the image consists of a sharp peak in the $k = 31$ cell and a two-cell-wide peak in the $k = 33$ and $k = 34$ cells, when $x_a = 6R + 31.425\Delta X$. As the target is translated even farther down-range by small fractions of ΔX, the $k = 33$ cell intensity decreases relative to the $k = 34$ cell intensity, as in figure 8e, until, in figure 8f, the image consists of two peaks of equal intensity in the $k = 31$ and $k = 34$ cells when $x_a = 6R + 31.5\Delta X$. This is the position for which point reflectors 0 and 1 are exactly in the center of the $k = 31$ and $k = 33$ cells, respectively. Translations of the target beyond $\Delta X/2$ give rise to image shapes that are either identical to or are mirror images of those for translations up to $\Delta X/2$.

We see from figures 8a through 8f that if two points have the same σ and are separated by $2\Delta X$, their images are easily distinguished, although there may be some ambiguity as to their actual separation and relative cross sections for some target locations. One may invoke the Rayleigh criterion for the resolution of two peaks, which requires that the minimum intensity between the peaks be no greater than one-half the peak intensity. Using this criterion, one may state that the two points of figure 8 are resolved as long as their down-range location differs from an integral number of ΔX by no more than $0.4\Delta X$.

In figures 6, 7, and 8, the reflectivities of both point reflectors are the same. One would expect that it would be more difficult to resolve two closely spaced point reflectors when the reflectivity of one is much larger than that of the other. This is illustrated in figure 9 (see pp 44–45), in which the point-reflectors are separated by $1.5\Delta X$, as in figure 7, but

Figure 8. Dependence of down-range image resolution of two points of equal reflectivity separated by 2.0 sampling cell lengths on location of points relative to a sampling cell edge: f_0 = 95 GHz, R = 15 m, ΔX = 0.234 m, $\rho_0 = \rho_1 = \rho$.

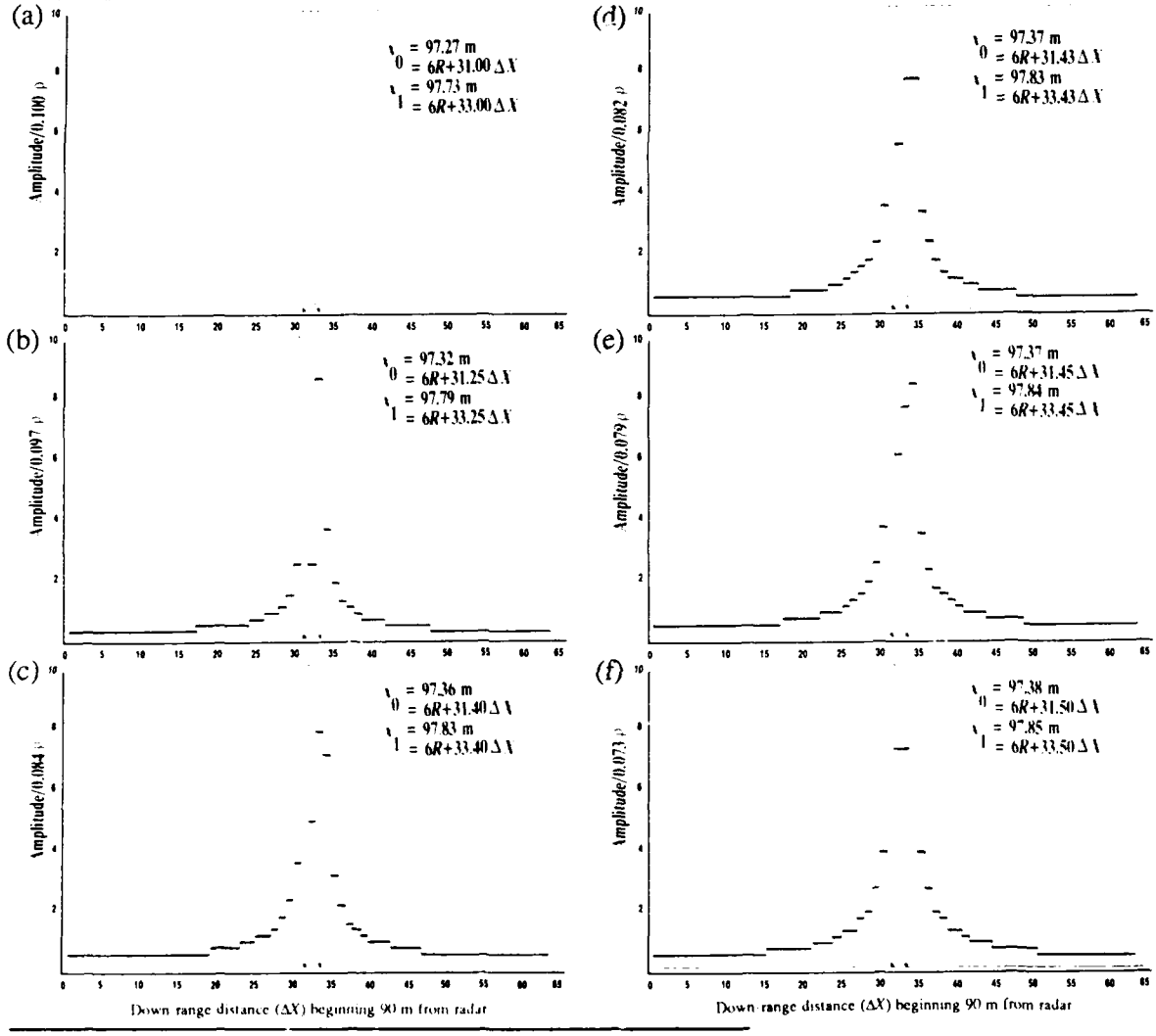

Fig.	f_0 (GHz)	x_0 (m)	Δx_0 (m)	x_1 (m)	Δx_1 (m)	$\frac{\rho_0}{\rho}$	$\frac{y_0}{\rho}$	$\frac{\rho_1}{\rho}$	$\frac{y_1}{\rho}$
8a	95	97.3	0.1	97.7	0.2	1.0	1.0	1.0	1.0
8b	95	97.3	0.1	97.1	0.1	1.0	1.0	1.0	0.8
8c	95	97.4	0.0	97.1	0.1	1.0	0.8	1.0	0.7
8d	95	97.4	0.0	97.2	0.2	1.0	0.8	1.0	0.6
8e	95	97.4	0.0	97.8	0.3	1.0	0.8	1.0	0.7
8f	95	97.4	0.0	97.9	0.2	1.0	0.7	1.0	0.7

$\rho_0 = \rho$ and $\rho_1 = 2\rho$. The figure shows the effect on the resolution of the two point reflectors as the location of point reflector 0 is varied from $6R + 32.0\Delta X$ through $6R + 32.5\Delta X$. It will be seen that for the range of target locations in figure 9, the two point reflectors are only resolved according to the Rayleigh criterion over the following ranges of point reflector 0 locations: a small interval around $6R + 32.185\Delta X$, $6R + 32.260\Delta X$ through $6R + 32.360\Delta X$, and $6R + 32.435\Delta X$ through $6R + 32.475\Delta X$. Thus the two point reflectors are resolved over virtually the entire range when their reflectivities are the same, as was seen in figure 7, but only over about 60 percent of the range when one has twice the reflectivity of the other.

Figure 9. Dependence of down-range image resolution and peak height ratio of two points having reflectivities in ratio 1 : 2 and separated by 1.5 sampling cell lengths on location of points relative to a sampling cell edge: $f_0 = 95$ GHz, $R = 15$ m, $\Delta X = 0.234$ m, $\rho_0 = \rho$, $\rho_1 = 2\rho$.

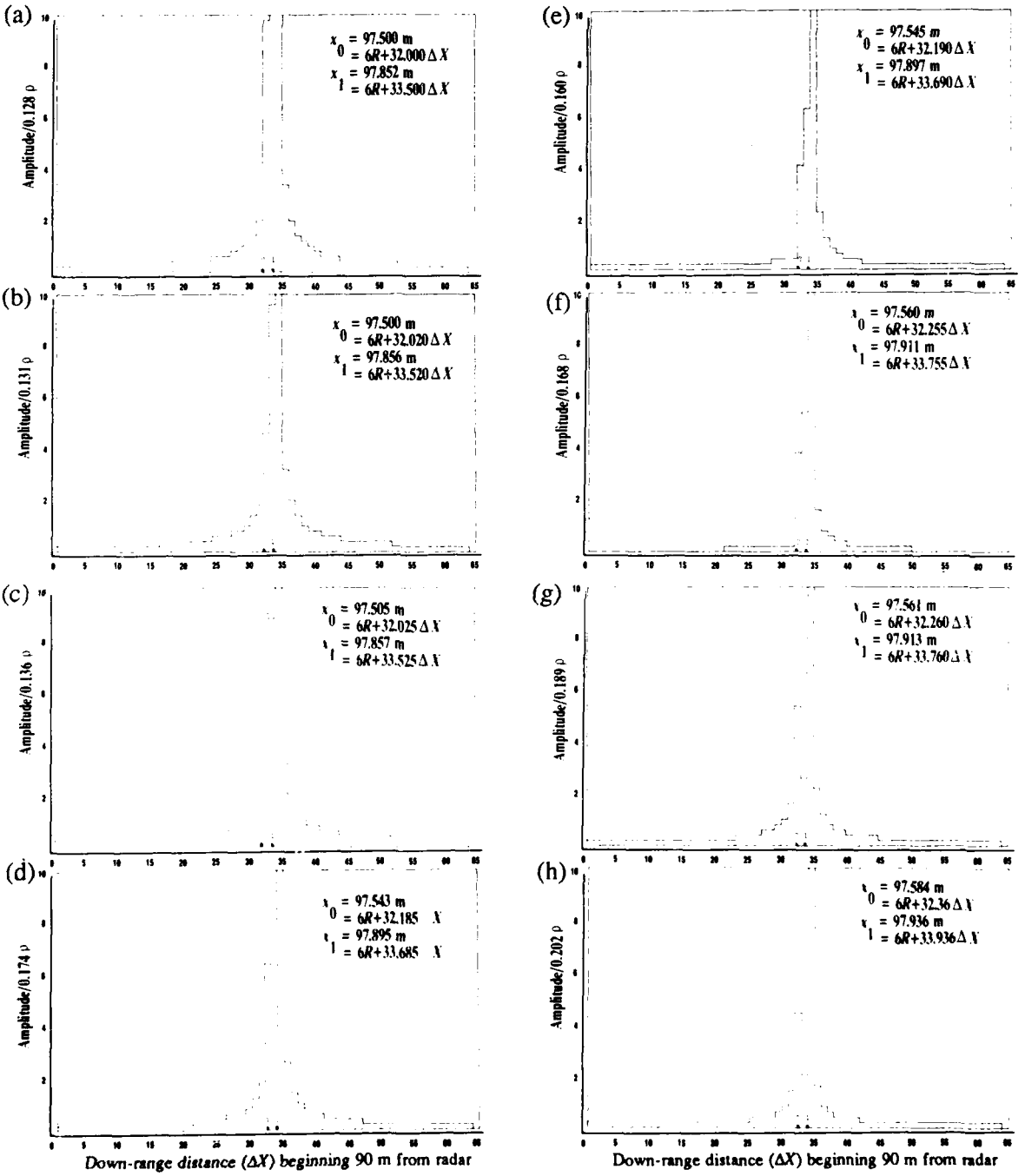

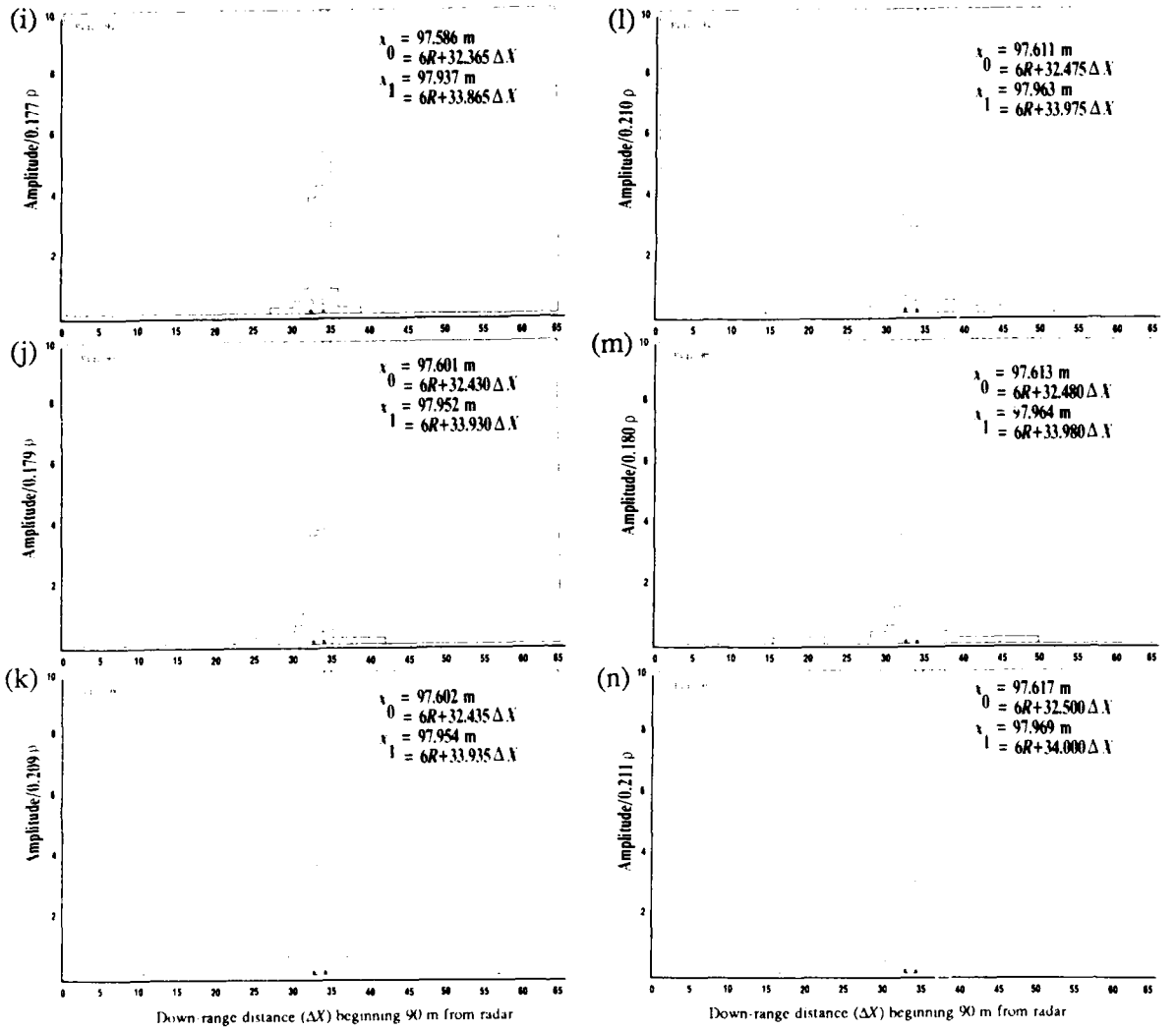

Fig.	f_0 (GHz)	x_0 (m)	Δx_0 (m)	x_1 (m)	Δx_1 (m)	$\frac{\rho_0}{\rho}$	$\frac{y_0}{\rho}$	$\frac{\rho_1}{\rho}$	$\frac{y_1}{\rho}$
9a	95	97.5	*	97.9	*	1.0	*	2.0	*
9b	95	97.5	*	97.9	*	1.0	*	2.0	*
9c	95	97.5	0.1	97.9	0.2	1.0	1.2	2.0	1.4
9d	95	97.5	0.1	97.9	0.2	1.0	1.1	2.0	1.7
9e	95	97.5	*	97.9	*	1.0	*	2.0	*
9f	95	97.6	*	97.9	*	1.0	*	2.0	*
9g	95	97.6	0.0	97.9	0.2	1.0	1.0	2.0	1.9
9h	95	97.6	0.0	97.9	0.2	1.0	0.9	2.0	2.0
9i	95	97.6	*	97.9	*	1.0	*	2.0	*
9j	95	97.6	*	98.0	*	1.0	*	2.0	*
9k	95	97.6	0.0	98.0	0.1	1.0	0.8	2.0	2.1
9l	95	97.6	0.0	98.0	0.1	1.0	0.7	2.0	2.1
9m	95	97.6	*	98.0	*	1.0	*	2.0	*
9n	95	97.6	*	98.0	*	1.0	*	2.0	*

14. Cross-Range Resolution and Two-Dimensional Images

The target images discussed in this report display only the variation of radar reflectivity along the down-range direction, irrespective of any cross-range variation in reflectivity. However, it may be shown[1] that if the target rotates about some axis through the target, then an image displaying the variation in radar reflectivity in the cross-range direction may be obtained. The cross-range resolution arises from the direct dependence of the rate of change of return signal phase on radius of rotation. This process turns out to be mathematically equivalent to achieving down-range resolution through the direct dependence of return signal phase on radar-to-target distance, which is discussed in this report. Hence, one may reasonably expect to be able to obtain images which resolve high-radar-reflectivity objects closely spaced in cross range. Finally, it may be shown that when the down-range and cross-range imaging processes are combined, one obtains two-dimensional images which yield information on both the relative position and reflectivity of closely spaced "glint points."

[1] *R. N. Trebits,* ***Synthetic Aperture Radar,*** *in* ***Principles of Modern Radar,*** *J. L. Eaves and E. K. Reedy, eds, Van Nostrand Reinhold (1987), pp 502–537.*

15. Summary and Conclusions

This report justifies representing the down-range image of a finite-size target by means of the magnitude of the DFT of the return signals from this target obtained by a stepped-frequency radar. It shows that as long as the target extension is less than the unambiguous range, R, of the radar, and the target lies entirely within one sampling interval of length R, the DFT magnitude sequence plotted in "normal" order is a useful representation of the target. If the target lies in two neighboring sampling intervals, its proper shape may be represented by the DFT-magnitude sequence plotted in some cyclic permutation from "normal" order. However, except for cases in which there is sufficient prior information about the target and its surroundings, the exact target location and shape cannot be determined unambiguously using these imaging methods. The report furthermore shows that the more closely the target resembles an ideal one, consisting of a discrete number of high-reflectivity objects of infinitesimal extent in the down-range direction, the more accurate is its representation by a DFT-magnitude sequence. It gives exact derivations of the down-range images for such ideal targets for radar frequencies of the order of 1 GHz to tens of gigahertz. Down-range images were computed and are displayed in histogram form for a variety of point scatterer positions, separations, and reflectivities. These computations show that it is possible to resolve all the point scatterers of the target, as long as they are separated by at least 1.5 down-range resolution cell lengths, and the ratios of their reflectivities are less than or equal to 2:1. In these cases the locations of the image peaks generally correspond to the actual locations of the scatterers within a down-range resolution cell length. The shapes of the histogram images, however, are fairly sensitive to the exact locations of the scatterers within a resolution cell. For this reason, some of the image histograms yield incorrect results for the relative reflectivities of the scatterers, even though the scatterers are resolved and imaged at the correct positions.

DISTRIBUTION

ADMINISTRATOR
DEFENSE TECHNICAL INFORMATION
CENTER
ATTN DTIC-DDA (2 COPIES)
CAMERON STATION, BUILDING 5
ALEXANDRIA, VA 22304-6145

DIRECTOR
US ARMY BALLISTIC RESEARCH
LABORATORY
ATTN DIRECTOR, SLCBR-D
ATTN SLCBR-SE-W, H. B. WALLACE
ABERDEEN PROVING GROUND, MD 21005

US ARMY ELECTRONIC TECHNOLOGY
& DEVICES LABORATORY
ATTN SLCET-DD
FT MONMOUTH, NJ 07703

DIRECTOR
US ARMY MATERIEL SYSTEMS
ANALYSIS ACTIVITY
ATTN AMXSY-MP
ABERDEEN PROVING GROUND, MD 21005

DEPT OF THE AIR FORCE, HQ
6585TH TEST GROUP (AFSC)
RADAR TARGET SCATTER FACILITY
ATTN LT COL RONALD L. KERCHER, CHIEF
HOLLOMAN AFB, NM 88330

ENGINEERING SOCIETIES LIBRARY
ATTN ACQUISITIONS DEPARTMENT
345 EAST 47TH STREET
NEW YORK, NY 10017

NATIONAL OCEANIC & ATMOSPHERIC ADM
ENVIRONMENTAL RESEARCH LABORATORIES
ATTN LIBRARY, R-51, TECH REPORTS
BOULDER, CO 80302

DIRECTOR
DEFENSE ADVANCED RESEARCH
PROJECTS AGENCY
ATTN TARGET ACQUISITION
& ENGAGEMENT DIV
1400 WILSON BLVD
ARLINGTON, VA 22209

DIRECTOR
NATIONAL SECURITY AGENCY
ATTN TECHNICAL LIBRARY
FT MEADE, MD 20755

UNDER SECRETARY OF DEFENSE
FOR RESEARCH & ENGINEERING
ATTN RESEARCH & ADVANCED TECH
WASHINGTON, DC 20301

DIRECTOR
APPLIED TECHNOLOGY LABORATORY
AVRADCOM
ATTN DAVDL-ATL-TSD, TECH LIBRARY
FT EUSTIS, VA 23604

COMMANDER
US ARMY ARMAMENT, MUNITIONS,
& CHEMICAL COMMAND
ATTN DRDAR-TDR, RESEARCH
& TECHNOLOGY
DOVER, NJ 07801-5001

COMMANDER/DIRECTOR
ATMOSPHERIC SCIENCES LABORATORY
ATTN DELAS-AS, ATMOSPHERIC SENSING
DIV
WHITE SANDS MISSILE RANGE, NM 88002

COMMANDER
US ARMY COLD REGIONS
RESEARCH & ENGINEERING LABORATORY
ATTN CRREL-TI, TECHNICAL INFO BR
HANOVER, NJ 03755

COMMANDER
CECOM
CENTER FOR EW/RSTA
ATTN AMSEL-RD-EW-R, ALAN TARBELL
FT MONMOUTH, NJ 07703-5300

COMMANDER
US ARMY MATERIEL COMMAND
ATTN AMCDM, DIR FOR PLANS & ANALYSIS
5001 EISENHOWER AVE
ALEXANDRIA, VA 22333-0001

DIRECTOR
US ARMY MISSILE LABORATORY
ATTN AMSMI-RPR, REDSTONE SCIENTIFIC
INFO CENTER
ATTN AMSMI-RPT, TECHNICAL INFORMATION
DIV
ATTN AMSMI-RD, SYS SIMULATION & DEV
DIR
ATTN AMSMI-RD, ADVANCED SENSORS DIR
ATTN AMSMI-RD-AS-MM, G. EMMONS
ATTN AMSMI-RD-AS-RA, J. LOOMIS
REDSTONE ARSENAL, AL 35809

DIRECTOR
NIGHT VISION & ELECTRO-OPTICS
CENTER
ATTN TECHNICAL LIBRARY
ATTN CNVEO-AC ADVANCED CONCEPTS
DIV
FT BELVOIR, VA 22060

DISTRIBUTION (cont'd)

US CHIEF ARMY RESEARCH OFFICE
(DURHAM)
ATTN DRXRO-EG, DIR ENGINEERING DIV
PO BOX 12211
RESEARCH TRIANGLE PARK, NC 27709

COMMANDER
US ARMY TEST & EVALUATION
COMMAND
ATTN STEWS-TE-LC (S. DICKERSON)
ATTN STEWS-TE-AG (F. MORENO)
WHITE SANDS MISSILE RANGE, NM 88002

DIRECTOR
NAVAL RESEARCH LABORATORY
ATTN 2600, TECHNICAL INFO DIV
WASHINGTON, DC 20375

COMMANDER
NAVAL SURFACE WARFARE CENTER
ATTN DX-21 LIBRARY DIV
DAHLGREN, VA 22448

COMMANDER
NAVAL SURFACE WARFARE CENTER
ATTN E-43, TECHNICAL LIB
WHITE OAK, MD 20910

COMMANDER
NAVAL WEAPONS CENTER
ATTN 38, RESEARCH DEPT
ATTN 381, PHYSICS DIV
CHINA LAKE, CA 93555

HEADQUARTERS
ARMAMENT DIV (AFSC)
ATTN MSD/ENL (MAJ M. TURK)
EGLIN AFB, FL 32542

DIRECTOR
NASA
GODDARD SPACE FLIGHT CENTER
ATTN 250, TECH INFO DIV
GREENBELT, MD 20771

DIRECTOR
NASA
LANGLEY RESEARCH CENTER
ATTN TECHNICAL LIBRARY
HAMPTON, VA 23665

ENVIRONMENTAL RESEARCH INSTITUTE
OF MICHIGAN
ATTN IRIA LIBRARY
PO BOX 618
ANN ARBOR, MI 48107

GEORGIA TECH RESEARCH INSTITUTE
GEORGIA INSTITUTE OF TECHNOLOGY
RADAR AND INSTRUMENTATION
LABORATORY
ATTN T. L. LANE
ATLANTA, GEORGIA 30332

LINCOLN LABORATORY
MASSACHUSETTS INSTITUTE OF
TECHNOLOGY
ATTN R. M. BARNES
LEXINGTON, MA 02173

SANDIA NATIONAL LABORATORIES
PO BOX 5800
ALBUQUERQUE, NM 87185

SIMULATION TECHNOLOGIES, INC.
ATTN A. V. SAYLOR
PO BOX 7009
HUNTSVILLE, AL 35807

TASC
ATTN K. L. WEEKS
907 MAR-WALT DRIVE
FORT WALTON BEACH, FL 32548

US ARMY LABORATORY COMMAND
ATTN TECHNICAL DIRECTOR, AMSLC-TD
ATTN DIRECTOR, AMCLD-S3 (N. BERG)

INSTALLATION SUPPORT ACTIVITY
ATTN LEGAL OFFICE, SLCIS-CC

USAISC
ATTN TECHNICAL REPORTS BRANCH,
AMSLC-IM-TR (2 COPIES)

HARRY DIAMOND LABORATORIES
ATTN D/DIVISION DIRECTOR
ATTN DIRECTOR, SLCHD-D
ATTN LIBRARY, SLCHD-TL (3 COPIES)
ATTN LIBRARY, SLCHD-TL (WOODBRIDGE)
ATTN CHIEF SCIENTIST, SLCHD-CS
ATTN DEPUTY DIRECTOR, SLCHD-DD
ATTN ASSOC DIRECTOR, SLCHD-PO
ATTN DIRECTOR, SLCHD-ST
ATTN DIRECTOR, SLCHD-NW
ATTN DIRECTOR, SLCHD-TA
ATTN DIRECTOR, SLCHD-TS
ATTN CHIEF, SLCHD-ST-AR
ATTN CHIEF, SLCHD-ST-SS
ATTN CHIEF, SLCHD-ST-MW
ATTN CHIEF, SLCHD-ST-OP
ATTN CHIEF, SLCHD-ST-SP
ATTN CHIEF, SLCHD-ST-R

DISTRIBUTION (cont'd)

HARRY DIAMOND LABORATORIES
(cont'd)
ATTN CHIEF, SLCHD-ST-SA
ATTN CHIEF, SLCHD-ST-MS
ATTN CHIEF, SLCHD-ST-AP
ATTN SLCHD-ST, P. WALKER
ATTN SLCHD-ST-AE, D. R. COOK
ATTN SLCHD-ST-MS, D. L. RODKEY (3 COPIES)
ATTN SLCHD-ST-SP, J. NEMARICH
ATTN SLCHD-ST-SP, R. WELLMAN
ATTN SLCHD-ST-SP, H. DROPKIN
ATTN SLCHD-ST-SP, J. SILVIOUS
ATTN SLCHD-ST-SP, G. GOLDMAN
ATTN SLCHD-ST-SP, D. WIKNER
ATTN SLCHD-ST-SP, D. HUTCHINS
ATTN SLCHD-ST-SS, M. PATTERSON
ATTN SLCHD-TA-ES, R. D. GOODMAN
ATTN SLCHD-ST-SP, J. SILVERSTEIN (25 COPIES)